J Anesth (2010) 24:225–233
DOI 10.1007/s00540-009-0831-7

ORIGINAL ARTICLE

Temporal profiles of aquaporin 4 expression and astrocyte response in the process of brain damage in fat embolism model in rats

Toru Gohara · Kazuyoshi Ishida · Kazuhiko Nakakimura · Mitsuyoshi Yoshida · Shiro Fukuda · Mishiya Matsumoto · Takefumi Sakabe

Received: 4 January 2009 / Accepted: 13 August 2009 / Published online: 29 January 2010

Abstract
Purpose Fat embolism syndrome is a serious complication observed after trauma, orthopedic surgery, and cardiac surgery. We investigated brain damage in relationship to temporal profiles of water channel aquaporin 4 (AQP4) and astrocyte response to fat embolism in rats.
Methods Triolein (2 μl) was injected into the right internal carotid artery in rats. Neurological outcome (score: range, 0–5 = no deficit–dead), brain water content, histopathology, and immunohistochemistry for AQP4 and glial fibrillary acidic protein (GFAP) were evaluated at 2 h (2 h group, $n = 12$), 24 h (24 h group, $n = 12$), and 72 h (72 h group, $n = 12$) after triolein injection. Saline was injected in the control (C) group ($n = 12$).
Results Neurological deficit score (median score of 2) and brain water content (mean value, 86.2%) increased significantly at 2 h with no progressive increase over 72 h. Damaged tissues with shrunken and triangular-shaped neurons with vacuole degeneration in cytoplasm and halo formation were distributed mainly, but not exclusively, to the ipsilateral hemisphere and were associated with increase in infiltration of inflammatory cells during the time course. Increases in immunostaining for AQP4 and GFAP were observed in the peri-affected region but not in the core. Reactive astrocytes with hypertrophy and dendrite elongation were detected at 72 h in the peri-affected region.
Conclusion The results suggest that brain damage with edema is induced very rapidly after triolein injection in association with increase in AQP4 expression and GFAP in the peri-affected region.

Keywords Fat embolism · Brain edema · Aquaporin 4 · Glial fibrillary acidic protein

T. Gohara · K. Ishida (✉) · K. Nakakimura · M. Yoshida · S. Fukuda · M. Matsumoto · T. Sakabe
Department of Anesthesiology, Yamaguchi University Graduate School of Medicine, 1-1-1 Minami-Kogushi, Ube, Yamaguchi 755-8505, Japan
e-mail: ishid002@yamaguchi-u.ac.jp

Introduction

Fat embolism syndrome has been known as one of the serious complications in trauma or orthopedic surgery, which presents high morbidity and mortality (5–15%) in severe cases [1, 2], leading to paresis, paralysis, convulsions, delirium, confusion, and stupor, which may deepen into coma [3–6]. Fat embolism has been recognized also as one of the most important types of embolism following cardiovascular surgery with cardiopulmonary bypass (CPB), leading to postoperative neurological dysfunction [7–9]. Even though filters are used in CPB devices, fat from bone marrow of the sternum, cardiac surface, and aortic wall is aspirated into the cardiotomy suction and then returned to the patient's circulation by way of the aortic cannula [7–9].

In animal experiments of fat embolism, cytotoxic and vasogenic brain edema has been recognized early after injection of triolein into the carotid arteries in rats [10] and cats [11–14]. However, limited information has been available concerning the brain pathology after fat embolism.

Recent studies have suggested that the water-selective membrane channel, aquaporin 4 (AQP4), is the primary route through which water moves in and out in response to osmotic change and plays an important role in astrocyte

swelling and brain edema formation and resolution in various pathological conditions, both in vitro [15, 16] and in vivo [17–23]. AQP4 is expressed throughout the brain, most preferentially in the perivascular astrocyte endfoot process and ependymal cells, and is suspected to be involved in brain edema formation. Because the astrocyte is also one of the major components of the blood–brain barrier (BBB) and plays an important role in both cytotoxic and vasogenic brain edema formation, it may be vital to evaluate astrocyte response in fat embolism.

Therefore, in the present study, we sought to investigate the temporal profiles of AQP4 expression and astrocyte response in the process of brain damage in the fat embolism model in rats.

Materials and methods

The protocol of this study was reviewed and approved by the Ethics Committee on Animal Experiment in Yamaguchi University Graduate School of Medicine.

Animals

Forty-eight male Wistar rats (weighing 280–320 g) were used. Rats were given free access to food and water and were housed in a 12-h:12-h light–dark cycle.

General preparation

Rats were anesthetized with 4% isoflurane. The tail artery was cannulated to monitor blood pressure, arterial blood gases, blood glucose, and hematocrit levels. After endotracheal intubation, lungs were mechanically ventilated with 2% isoflurane. A temperature probe was placed on the skull under the right temporal muscle and the cranial temperature was monitored (Mono-a-therm 6510; Mallinckrodt Japan, Tokyo, Japan) and maintained at 37 ± 0.1°C with external heating or cooling throughout the experiments. Rats were randomly assigned to the control (C) group ($n = 12$) and the fat embolism (triolein) group ($n = 36$). Because triolein was proved as a major constituent of fat in the bone marrow of lower extremities and adipocytes in humans [24, 25], we used triolein to represent emboli of fat in the present study. Rats of the triolein group were further assigned to three subgroups depending on the time schedule for the final evaluation after triolein injection: 2 h after triolein injection (2 h group, $n = 12$), 24 h after triolein injection (24 h group, $n = 12$), and 72 h after triolein injection (72 h group, $n = 12$). The rats of the C group were injected with the same volume of saline instead of triolein and evaluated 2 h after injection.

Fat embolism model

The right common carotid artery was exposed through a midline neck incision; the right external and internal carotid arteries were isolated, the occipital, the pterygopalatin, and the superior thyroid arteries were ligated, and a polyethylene catheter with an external diameter of 0.61 mm (PE10) was retrogradely introduced into the right external carotid artery so that its tip was placed adjacent to the still patent internal carotid artery. Every surgical wound was infiltrated with 0.5% bupivacaine. After a stabilization period of at least 10 min while anesthesia was maintained with 1.5% isoflurane and 40% O_2 in N_2, 2 μl 99% triolein was injected using a microsyringe over a period of 5 min through the polyethylene catheter. In our preliminary study, we tested several doses of triolein and found that 3 μl or a larger dose injected into the right internal carotid artery caused high mortality (70–90% of rats died 2–72 h after injection). Therefore, in the present study, we selected a dose of 2 μl. Following the injection of triolein, the catheter was removed; the neck incision sutured, and anesthetic administration was discontinued. The endotracheal tube was removed when spontaneous ventilation became adequate. Thereafter, the rats were returned to a plastic box insufflated with 3 l min^{-1} O_2 and were observed for 30 min, and then returned to their regular housing cage.

Neurological evaluation

Neurological evaluation was performed at the scheduled time for the final evaluation: 2, 24, and 72 h after triolein injection or 2 h after saline injection. The neurological findings were scored by an observer unaware of the treatment group using a six-point scale as described by Xiong et al. [26]: 0, no deficit; 1, failure to extend left forepaw fully; 2, circling to the left; 3, falling to the left; 4, no spontaneous walking, with a depressed level of consciousness; 5, dead.

Measurement of brain water content

After neurological evaluation at the predetermined time point, seven rats of each group were reanesthetized with isoflurane, intubated, and mechanically ventilated. Rats were then decapitated and their brains were rapidly removed. The brain was dissected into cortex (right/left), subcortex (right/left), and cerebellum, and water content of these sections was measured using the wet weight/dry weight method. The tissue samples were immediately weighed on an electronic analytical balance to obtain the wet weight (WW). The samples were then dried in an oven at 110°C for 24 h and weighed again to obtain the dry

weight (DW). The formula (WW – DW) × WW^{-1} × 100 was employed to calculate water content.

Histopathology and immunohistochemistry

Five rats of each triolein and C group were transcardially perfused and fixed with 10% phosphate-buffered formalin and embedded in paraffin. Coronal sections (8 μm thickness) of the brain were stained with hematoxylin and eosin (H&E). Three sections (–1.7, 3.8, and 7.8 mm caudal from the bregma) were chosen for evaluating the area of the lesions. The area of the lesions was determined with the aid of a microscope and image analyzer (Densitograph AE-6905C; Atto, Tokyo, Japan). The image of each section was stored and analyzed using the NIH image. Areas of the lesions of three sections of each rat were summarized.

Immunostaining for AQP4, for glial fibrillary acidic protein (GFAP), and combined staining were performed in the section 3.8 mm caudal from the bregma where the damage appeared most consistent. The sections were deparaffinized using xylene and ethanol. Endogenous peroxidase was inactivated using 3% hydrogen peroxide in methanol. After rinsing in phosphate-buffered saline (pH 7.2, 0.1 mol l^{-1}), nonspecific protein binding was blocked with 10% normal goat serum. The sections were incubated for 12 h with antibodies against AQP4 (rabbit antirat AQP4 affinity purified polyclonal antibody; Chemicon, Temecula, CA, USA) and with antibodies against GFAP (mouse anti-GFAP monoclonal antibody; Chemicon, Temecula, CA, USA) at 4°C. Antibody dilutions in phosphate-buffered saline for AQP4 and for GFAP were 1:250 and 1:200, respectively; this was followed by incubation with a second antibody [Histofine simple stain MAX-PO (M) or PO (R); Nichirei, Tokyo, Japan] at room temperature for 30 min. The sections were visualized with 3,3-diaminobenzidine hydrochloride (Histofine simple stain DAB; Nichirei) and then counterstained with hematoxylin.

Combined immunostaining of AQP4 and GFAP was done as follows. After visualization of the second antibodies against AQP4 with 3,3-diaminobenzidine hydrochloride (Histofine simple stain DAB; Nichirei), the sections were again rinsed in phosphate-buffered saline and incubated for 12 h with antibodies against GFAP (mouse anti-GFAP monoclonal antibody; Chemicon) at 4°C. This step was followed by incubation with a second antibody [Histofine simple stain AP (M); Nichirei] at room temperature for 30 min. The sections were revisualized with fukushin (new fukushin kit; Nichirei) and then counterstained with hematoxylin. Histopathological and immunohistochemical evaluation was performed by an observer unaware of the treatment groups. The intensity of AQP4 immunostaining was scored using the four-point scale: 0 = none, 1 = weak, 2 = moderate, and 3 = strong. The astrocytic response was scored using the five-point grading scale as described previously: 0 = nil, 1 = partial/weak, 2 = mild, 3 = moderate, and 4 = strong [27]. A distinct GFAP staining without astrocyte hypertrophy was rated as moderate (score 3), and an intense GFAP staining with astrocyte hypertrophy was rated as strong (score 4) [27].

Statistical analysis

Repeated-measures analysis of variance (ANOVA) was used to evaluate the differences in physiological parameters, and one-factorial ANOVA was used for evaluation of brain water content and area of the lesions followed by the Scheffé test. The unpaired *t* test was used to evaluate the difference of water content of both sides of the brain within groups. Neurological scores and immunohistochemical scores were analyzed with the Kruskal–Wallis test followed by the Mann–Whitney *U* test. $P < 0.05$ was considered statistically significant.

Results

Physiological variables in each experimental group are presented in Table 1. There were no significant differences among the groups.

Neurological outcome

All rats survived for the prescheduled time. The results are summarized in Table 2. Neurological deficit scores of the three triolein groups were significantly higher than those of the C group. There were no significant differences in neurological deficit scores among the three triolein groups.

Brain water content

Brain water content is shown in Fig. 1. In the three triolein groups, water content in the ipsilateral cortex and subcortex was significantly higher than that of the C group, but there were no significant time-dependent changes. There were no significant changes of water content in the contralateral cortex, subcortex, and cerebellum.

Histopathology and immunohistochemistry

The extent of the lesion at the level of –1.7, 3.8, and 7.8 mm caudal from bregma is illustrated in Fig. 2. Micrographs with low magnification of the brain slice 3.8 mm caudal from the bregma in each group are shown in Fig. 3. In the triolein groups, the lesion was mainly distributed in the ipsilateral parietal cortex and subcortex,

Table 1 Physiological variables

Group	MAP (mmHg)	pH	PaO_2 (mmHg)	$PaCO_2$ (mmHg)	Glucose (mg/dl)	Hematocrit (%)
Control ($n = 12$)						
Preinjection	97 ± 15	7.46 ± 0.02	170 ± 16	40 ± 2	185 ± 33	38 ± 2
Postinjection	94 ± 9	7.46 ± 0.03	175 ± 18	39 ± 2	173 ± 23	38 ± 2
Triolein 2 h ($n = 12$)						
Preinjection	101 ± 10	7.45 ± 0.02	173 ± 15	40 ± 1	190 ± 24	38 ± 3
Postinjection	104 ± 9	7.44 ± 0.03	174 ± 17	39 ± 2	172 ± 18	38 ± 3
24 h ($n = 12$)						
Preinjection	96 ± 11	7.46 ± 0.02	180 ± 13	39 ± 1	183 ± 11	39 ± 3
Postinjection	99 ± 11	7.45 ± 0.02	184 ± 14	39 ± 2	172 ± 13	37 ± 3
72 h ($n = 12$)						
Preinjection	103 ± 18	7.46 ± 0.01	172 ± 11	39 ± 1	189 ± 23	39 ± 2
Postinjection	104 ± 13	7.45 ± 0.02	174 ± 14	40 ± 2	170 ± 21	38 ± 1

Values are expressed as mean ± SD

MAP, mean arterial pressure

Table 2 Neurological outcome

Group	Neurological deficit score					
	0	1	2	3	4	5
Control	11	1	0	0	0	0
Triolein						
2 h*	0	3	7	2	0	0
24 h*	0	5	3	4	0	0
72 h*	0	5	3	4	0	0

Values are expressed as numbers of rats

* $P < 0.05$ versus control

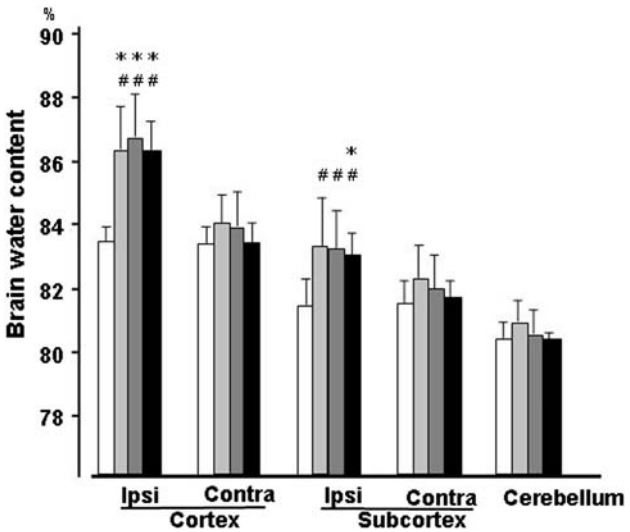

Fig. 1 Brain water content of ipsilateral and contralateral cortex, subcortex, and cerebellum in each group. Values were expressed as mean ± standard deviation. In three triolein groups (*light gray bars*, 2 h group; *gray bars*, 24 h group; *black bars*, 72 h group), water content in the ipsilateral cortex and subcortex was significantly higher than that of the control group (*white bars*), but there were no significant differences among the three triolein groups. There were no significant changes of water content in the contralateral cortex, subcortex, and cerebellum. *Ipsi*, ipsilateral side; *Contra*, contralateral side. $^{*}P < 0.05$ versus control group; $^{\#}P < 0.05$ versus contra

including hippocampus and thalamus, but small lesions were detected also in the contralateral parietal cortex in some animals.

The total area of the lesion of three sections of each rat in each triolein group (2, 24, and 72 h) was 31 ± 11, 35 ± 15, and 36 ± 5 mm^2 with no intergroup difference.

Micrographs of H&E staining with high magnification of the area indicated by an arrow in each corresponding view with low magnification in Fig. 3 are shown in Fig. 4a–g. In the 2 h triolein group, shrunken and triangular-shaped neurons with cytoplasmic eosinophilia, Nissl body disappearance, and pyknotic nucleus were prominent. Vacuole degeneration in cytoplasm and halo formation around the neurons and small vessels were observed in the core lesion (Fig. 4b). In the 24 h triolein group, pyknosis or disappearance of the nucleus and vacuole degeneration in the cytoplasm was more severe (Fig. 4d). In the 72 h triolein group, the lesion became more prominent with inflammatory infiltrated cells (Fig. 4f).

Figure 4h–n shows micrographs of AQP4 immunostaining. In the C group, AQP4 was weakly stained in the perivascular area (Fig. 4h). In the triolein groups, no immunoactivity of AQP4 was observed in the core of the lesion (Fig. 4i,k,m). In the peri-affected region surrounding the core of the lesion, AQP4 immunostaining was high in all triolein groups (Fig. 4j,l,n). In the region with high AQP4 immunostaining, both neurons with fewer pyknotic changes and those with a normal appearance were seen.

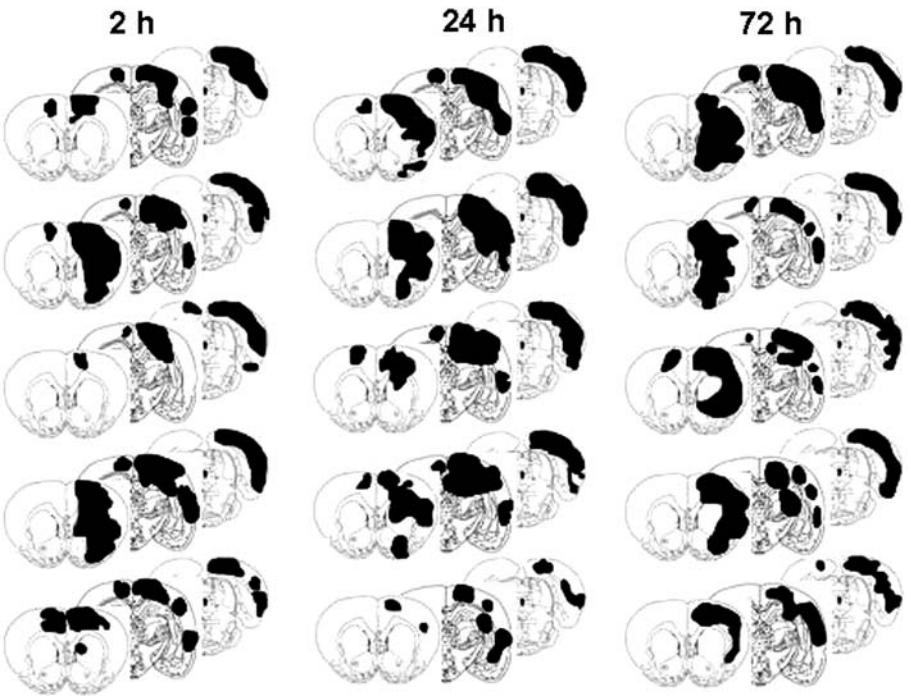

Fig. 2 Schematic illustration of the extent of lesion at the level of –1.7, 3.8, and 7.8 mm caudal from bregma in each rat of three triolein groups. In the triolein groups, the lesions were mainly distributed in the ipsilateral parietal cortex and subcortex, including hippocampus and thalamus, but small lesions were detected also in the contralateral parietal cortex in some animals

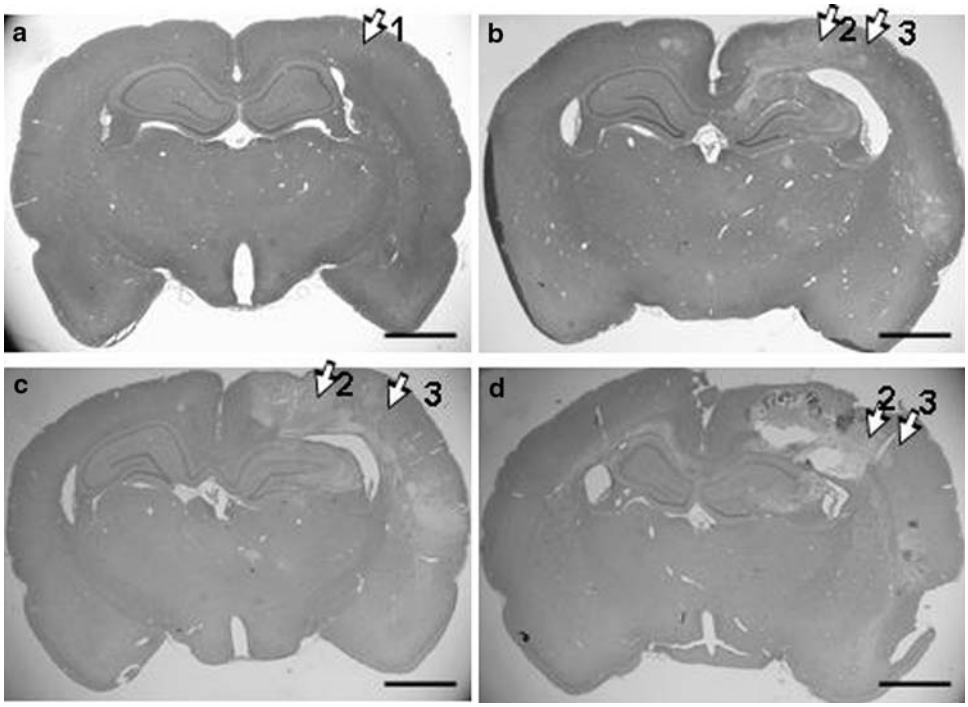

Fig. 3 Micrographs of the brain section 3.8 mm caudal from the bregma with hematoxylin and eosin (H&E) staining. **a** Control group; **b** 2 h group; **c** 24 h group; **d** 72 h group. Three arrows (*arrow 1*, control; *arrow 2*, core lesion; *arrow 3*, peri-affected region) correspond to Fig. 4. In the triolein groups, the lesions were mainly distributed in the ipsilateral parietal cortex and subcortex, including hippocampus and thalamus, but small lesions were detected also in the contralateral parietal cortex (*Bars* **a**–**d** 2 mm)

Figure 5 shows the scores of immunostaining of AQP4. In the C group, the immunostaining score of AQP4 was 1, whereas in the triolein groups the AQP4 immunostaining score was 0 in the core of the lesion, but was as high as score 2 or 3 in the peri-affected region.

Micrographs of GFAP immunostaining are shown in Fig. 4o–v. In the C group, no apparent GFAP-stained cells were observed (Fig. 4o). In the triolein groups, GFAP immunostaining was nil or weak in the core of the lesion (Fig. 4p,r,t). The GFAP staining was high in the peri-affected region in the 2 h and 24 h groups (Fig. 4q,s). In the 72 h group, GFAP immunostaining became intense with hypertrophy and dendrite elongation of astrocytes (Fig. 4u,v). In the region with high GFAP immunostaining,

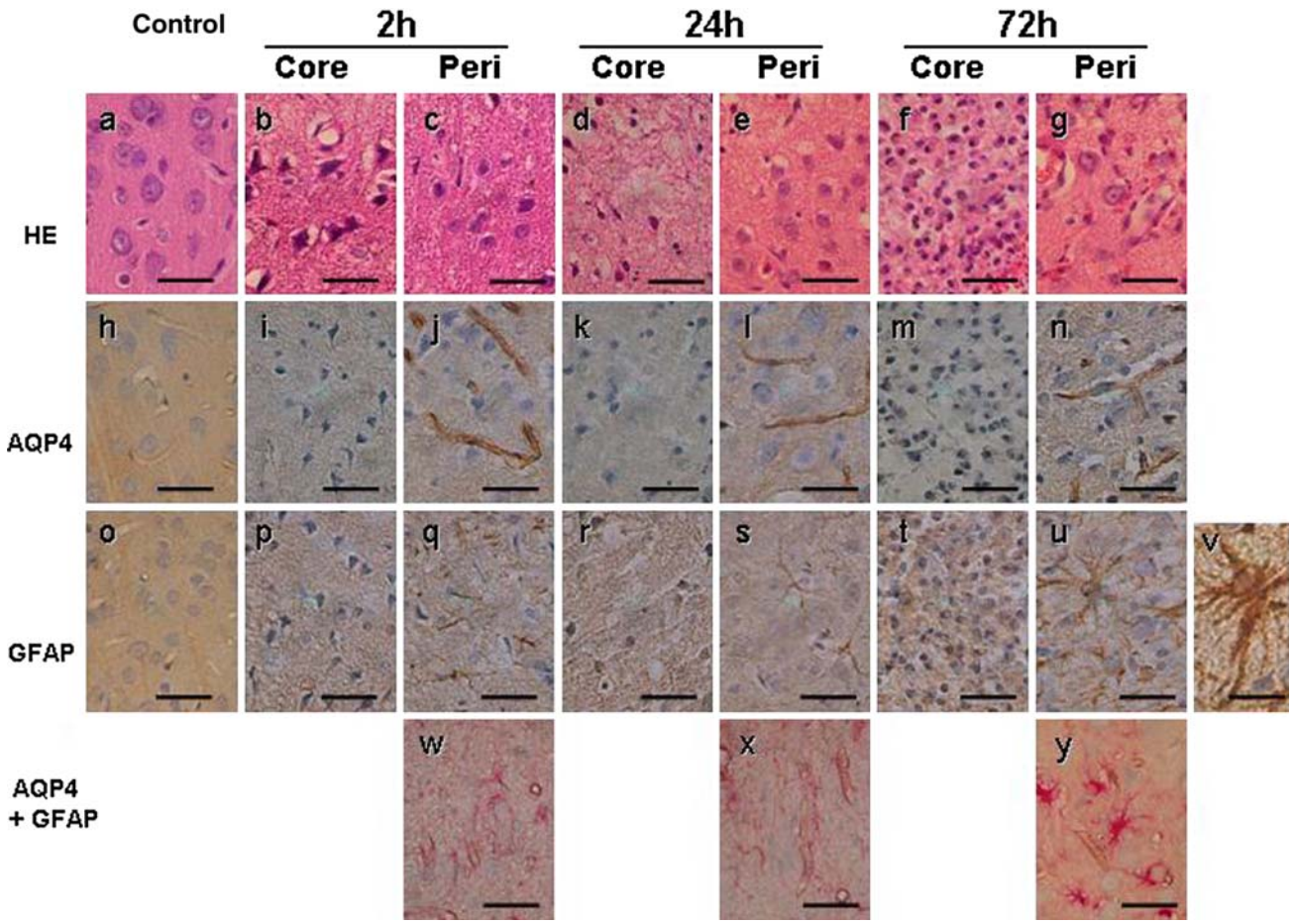

Fig. 4 Micrographs of brain sections 3.8 mm caudal from the bregma with high magnification of the area indicated by *arrows* in the corresponding areas with low magnification in Fig. 3. **a**–**g** Hematoxylin and eosin (H&E; *HE*) staining: In the 2 h group, shrunken and triangular-shaped neurons with cytoplasmic eosinophilia, Nissl body disappearance, and pyknotic nucleus were prominent. Vacuole degeneration in cytoplasm and halo formation around the neurons and small vessels were observed in the core (**b**). In the peri-affected region in the 2 h group, both abnormally shaped neurons with halo formation but fewer pyknotic and normal appearance neurons existed (**c**). In the core of the lesion of the 24 h group, pyknosis or disappearance of nucleus and vacuole degeneration in the cytoplasm was more severe (**d**). In the peri-affected region of the 24 h group, both neurons with pyknosis or disappearance of nucleus and neurons with normal appearance nucleus and slight halo formation were observed (**e**). In the core of the 72 h group, the lesion became more prominent with inflammatory infiltrated cells in the core (**f**). In the peri-affected region of the 72 h group, mild infiltration of inflammatory cells and neurons with normal appearance were observed (**g**). **h**–**n** Aquaporin 4 (*AQP4*) staining: in the control group, AQP4 was weakly stained in the perivascular area (**h**). In the triolein groups, no immunoactivity of AQP4 was observed in the core of the lesion (**i**, **k**, **m**). In the peri-affected region surrounding the core of the lesion, AQP4 immunostaining was high in all triolein groups (**j**, **l**, **n**). **o**–**v** Glial fibrillary acidic protein (*GFAP*) staining: in the control group, no apparent GFAP-stained cells were observed (**o**). In the triolein groups, GFAP immunostaining was nil or weak in the core of the lesion (**p**, **r**, **t**). GFAP staining was high in peri-affected region in the 2 h (**q**) and 24 h (**s**) groups. In the 72 h group, GFAP immunostaining became intense (**u**, **v**). **v** High magnification of astrocyte hypertrophy and dendrite elongation. **w**–**y** Combined immunostaining of AQP4 and GFAP in the 2, 24, and 72 h groups: AQP4 was stained brown by histofine and GFAP was stained red by fukushin. The areas of increased immunostaining in AQP4 and GFAP were colocalized. *Bars* **a**–**u**, **w**–**y** 25 μm; **v** 12.5 μm)

both neurons with fewer pyknotic changes and those with a normal appearance were seen.

Figure 6 shows the scores of immunostaining of GFAP. In the C group, the GFAP immunostaining score was 0, whereas in the triolein groups, the GFAP immunostaining score was 0 or 1 in the core of the lesion, but was high (score 1–4) in the peri-affected region. Four sections of brain in the 72 h triolein group were scored as 4 with hypertrophy and dendrite elongation of astrocytes.

Combined immunostaining of AQP4 and GFAP in the peri-affected lesion of the 2, 24, and 72 h group is shown in Fig. 4w–y. The combined immunostaining of AQP4 and GFAP was seen in astrocytes. The areas of increased immunostaining in AQP4 and GFAP were colocalized. A similar staining pattern was observed in all triolein groups.

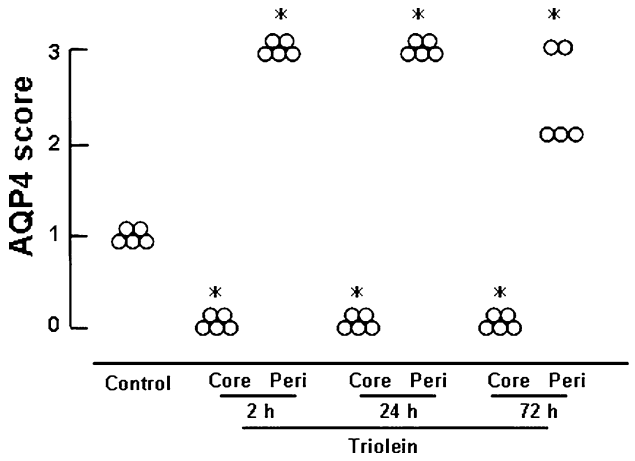

Fig. 5 Scores of immunostaining of *AQP4* in each group in the section 3.8 mm caudal from the bregma. In the *Control* group, the immunostaining score of AQP4 was 1; in the triolein groups, the AQP4 immunostaining score was 0 in the core of the lesion but was as high as 2 or 3 in the peri-affected region. $*P < 0.05$ versus Control group

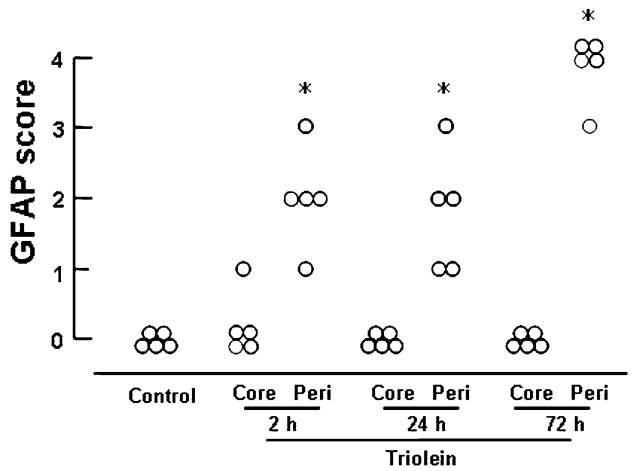

Fig. 6 Scores of immunostaining of *GFAP* in the section 3.8 mm caudal from the bregma. In the *Control* group, the GFAP immunostaining score was 0; in the triolein groups, the GFAP immunostaining score was 0 or 1 in the core of the lesion, but was high (score 1–4) in the peri-affected region. Four sections in the 72 h group were scored 4 with dendrite elongation and hypertrophy of astrocytes. $*P < 0.05$ versus Control group

Discussion

In the present study we found that (1) neurological deficit score and brain water content almost reached a peak at 2 h after intracarotid injection of triolein with no progressive deterioration over 72 h; (2) histological damage was distributed mainly, although not exclusively, to the ipsilateral hemisphere with a time-dependent increase in inflammatory cell infiltration without enlargement of damaged area; (3) increases in immunostaining for AQP4 and GFAP were observed in the peri-affected region but not in the core; and (4) reactive astrocytes were present with hypertrophy and dendrite elongation at 72 h after triolein injection. The results suggest that brain damage with an increase in brain water content and neurological dysfunction can be induced very rapidly if a certain amount of fat is introduced into the cerebral circulation.

Histological damage was characterized by vacuole degeneration of the cytoplasm and halo formation around neurons and small vessels in the core of the lesion. These changes have been known to represent astrocyte swelling and cytotoxic brain edema [28]. However, there has been a study that showed early occurrence of BBB disruption detected by ^{99m}Tc uptake to the brain 15 or 30 min after triolein injection in rats [10], suggesting that a vasogenic cause may also contribute, in part, to edema formation after fat embolism. Kim et al. [12] have reported that two types of lesions were detected by magnetic resonance imaging (MRI) 30 min after triolein injection in cats. The type 1 lesion had hyperintensity on diffusion-weighted images and mild enhancement on contrast-enhanced T_1-weighted images, corresponding to both cytotoxic and vasogenic edema. The type 2 lesion had iso- or mild hyperintensity on diffusion-weighted images and strong enhancement on contrast-enhanced T_1-weighted images corresponding to vasogenic edema. This type 2 lesion frequently surrounded the type 1 lesion and returned to a normal appearance within 2–3 weeks [12, 13]. It may be possible that, in the peri-affected region surrounding the core lesion, a vasogenic cause may, at least in part, have contributed to edema formation and that both cytotoxic and vasogenic brain edema can occur early after fat embolism.

We observed marked increases in immunostaining for AQP4 and GFAP in the peri-affected region but not in the core. It is not clear why the GFAP score tended to show a gradual increase compared to AQP4. However, we think that it requires time for astrocytes to show typical morphological changes, hypertrophy, and dendrite elongation [27, 29–31]. AQP4 has been known to express in the perivascular astrocyte endfoot process. Our findings are in good agreement with the close correlation between levels of AQP4 mRNA and the density of GFAP in astrocytes 6 days after brain injury induced by injection of quinolinic acid reported by Vizuete et al. [17]. The functional role of AQP4, although not yet fully understood, seems to differ depending on the type of brain injury: in water intoxication and focal ischemia (both presenting with cytotoxic edema), AQP4 knockout mice exhibited significantly less brain edema with improvement of neurological status and survival rate compared with the wild type [19], whereas, in the continuous intracerebral fluid infusion (vasogenic edema) model, AQP4 knockout mice developed higher intracranial pressure (ICP) in association with higher brain water content compared with wild-type controls [21]. In the

present study, brain edema formation was rapid and almost reached a peak within 2 h after triolein injection in association with astrocyte swelling and morphological changes (hypertrophy) over time in the peri-affected regions. In contrast, in the core, the damage was very severe and both AQP4 and astrocyte (GFAP staining) have not been detected. We speculate that the peri-affected region with increased immunostaining for AQP4 and GFAP represents a type 2 lesion where vasogenic edema is dominant and can be resolved over time, as reported by Kim et al. [13]. High immunostaining for AQP4 may have contributed to resolution of brain edema because brain edema was not progressive during the time course in the present study.

The role of reactive astrocytes is complex and appears to be double edged, either protective or deteriorative. For example, reactive astrocytes provide trophic substances and transcription genes to reduce neuronal damage [32] and also to promote repair of the BBB through production of extracellular matrix components [33]. GFAP null mice have been shown to have high susceptibility to cerebral ischemia [34]. Further, a recent report shows that AQP4 contributes to the astrocyte migration and glial scar formation [35]. In the cortical-stab-injury model, glial scar formation was less in the AQP4 knockout mouse than the wild type [35]. The results suggest that an increase in AQP4 associated with astrocyte activation (GFAP increase) may lead to repair of injury. In contrast, reactive astrocytes have been reported to play an important role in the occurrence of delayed expansion of infarct volume, possibly by producing S-100β protein and activating inducible nitric oxide synthase in focal brain ischemia [36]. Pharmacological modulation of astrocytic activation mitigates delayed expansion of infarct volume after middle cerebral artery occlusion [37]. In the present study, because the damaged areas were not enlarged over time, it is speculated that the reactive astrocytes in the peri-affected region may have provided a protective effect.

Immunostaining cannot distinguish the transcriptionally or translationally upregulated AQP4 and the facilitated membrane presentation of AQP4. In the present study, robust AQP4 expression was observed 2 h after triolein injection, and the results were in accordance with the recent report that showed rapid increase in AQP4 immunostaining 1 h after ischemia with increased protein expression [38]. The upregulation of mRNA and increased protein expression of AQP4 were simultaneously seen 3 h after hypoxia [39]. Therefore, it is conceivable, although it may not be conclusive, that mRNA of AQP4 may be also upregulated.

In summary, the present study demonstrated that brain damage with fat embolism is characterized by early formation of severe brain edema, associated with an increase in AQP4 expression and GFAP in the peri-affected region but with no presence in the core. Although the functional role of observed temporal profiles of AQP4 and astrocyte responses remains to be elucidated, early modulation of AQP4 and astrocyte responses can be one of the targets for the treatment of fat embolism syndrome.

Acknowledgments This study was supported in part by a grant-in-aid for scientific research (grant no. 12671474), the Japanese Ministry of Education, Culture, Sports and Technology.

References

1. Johnson MJ, Lucas GL. Fat embolism syndrome. Orthopedics. 1996;19:41–9.
2. Bulger EM, Smith DG, Maier RV, Jurkovich GJ. Fat embolism syndrome. A 10-year review. Arch Surg. 1997;132:435–9.
3. Meeke RI, Fitzpatrick GJ, Phelan DM. Cerebral oedema and the fat embolism syndrome. Intensive Care Med. 1987;13:291–2.
4. di Summa A, Beltramello A, Fratucello GB, Bongiovanni LG, Zanette G, Polo A. Cerebral fat embolism: debated acute post-traumatic encephalography. Eur Neurol. 1998;40:55–6.
5. Prentiss JE, Imoto EM. Fat embolism, ARDS, coma, death: the four horsemen of the fractured hip. Hawaii Med J. 2001;60:15–9.
6. Kariya N, Shindoh M, Hayashi Y, Nakasuji M, Nishi S, Nishikawa K, et al. A case of fatal paradoxical fat embolism syndrome detected by intraoperative transesophageal echocardiography. Anesth Analg. 2001;92:688–9.
7. Ghatak NR, Sinnenberg RJ, deBlois GG. Cerebral fat embolism following cardiac surgery. Stroke. 1983;14:619–21.
8. Brown WR, Moody DM, Challa VR. Cerebral fat embolism from cardiopulmonary bypass. J Neuropathol Exp Neurol. 1999;58:109–19.
9. Hammon JW, Stump DA, Butterworth JB, Moody DM. Approaches to reduce neurologic complications during cardiac surgery. Semin Thorac Cardiovasc Surg. 2001;13:184–91.
10. Drew PA, Smith E, Thomas PD. Fat distribution and changes in the blood–brain barrier in a rat model of cerebral arterial fat embolism. J Neurol Sci. 1998;156:138–43.
11. Kim HJ, Lee CH, Lee SH, Cho BM, Kim HK, Park BR, et al. Early development of vasogenic edema in experimental cerebral fat embolism in cats: correlation with MRI and electron microscopic findings. Invest Radiol. 2001;36:460–9.
12. Kim HJ, Lee JH, Lee CH, Lee SH, Moon TY, Cho BM, et al. Experimental cerebral fat embolism: embolic effects of triolein and oleic acid depicted by MR imaging and electron microscopy. Am J Neuroradiol. 2002;23:1516–23.
13. Kim HJ, Lee CH, Lee SH, Moon TY. Magnetic resonance imaging and histologic findings of experimental cerebral fat embolism. Invest Radiol. 2003;38:625–34.
14. Kim YW, Kim HJ, Cho BM, Moon TY, Eun CK. The study of cerebral hemodynamics in the hyperacute stage of fat embolism induced by triolein emulsion. Am J Neuroradiol. 2006;27:398–401.
15. Yamamoto N, Yoneda K, Asai K, Sobue K, Tada T, Fujita Y, et al. Alterations in the expression of the AQP family in cultured rat astrocytes during hypoxia and reoxygenation. Brain Res Mol Brain Res. 2001;90:26–38.
16. Arima H, Yamamoto N, Sobue K, Umenishi F, Tada T, Katsuya H, et al. Hyperosmolar mannitol simulates expression of aquaporins 4 and 9 through a p38 mitogen-activated protein kinase-dependent pathway in rat astrocytes. J Biol Chem. 2003;278:44525–34.

17. Vizuete ML, Venero JL, Vargas C, Ilundain AA, Echevarria M, Machado A, et al. Differential upregulation of aquaporin-4 mRNA expression in reactive astrocytes after brain injury: potential role in brain edema. Neurobiol Dis. 1999;6:245–58.
18. Taniguchi M, Yamashita T, Kumura E, Tamatani M, Kobayashi A, Yokawa T, et al. Induction of aquaporin-4 water channel mRNA after focal cerebral ischemia in rat. Brain Res Mol Brain Res. 2000;78:131–7.
19. Manley GT, Fujimura M, Ma T, Noshita N, Filiz F, Bollen AW, et al. Aquaporin-4 deletion in mice reduces brain edema after acute water intoxication and ischemic stroke. Nat Med. 2000;6:159–63.
20. Ke C, Poon WS, Ng HK, Pang JC, Chan Y. Heterogeneous responses of aquaporin-4 in oedema formation in a replicated severe traumatic brain injury model in rats. Neurosci Lett. 2001;301:21–4.
21. Papadopoulos MC, Manley GT, Krishna S, Verkman AS. Aquaporin-4 facilitates reabsorption of excess fluid in vasogenic brain edema. FASEB J. 2004;18:1291–3.
22. Papadopoulos MC, Verkman AS. Aquaporin-4 gene disruption in mice reduces brain swelling and mortality in pneumococcal meningitis. J Biol Chem. 2005;280:13906–12.
23. Mao X, Enno TL, Del Bigio MR. Aquaporin 4 changes in rat brain with severe hydrocephalus. Eur J Neurosci. 2006;23:2929–36.
24. Djelouah I, Lefevre G, Ozier Y, Rosencher N, Tallet F. Fat embolism in orthopedic surgery: role of bone marrow fatty acid. Anesth Analg. 1997;85:441–3.
25. Insull W Jr, Bartsch GE. Fatty acid composition of human adipose tissue related to age, sex, and race. Am J Clin Nutr. 1967;20:13–23.
26. Xiong L, Zheng Y, Wu M, Hou L, Zhu Z, Zhang X, et al. Preconditioning with isoflurane produces dose-dependent neuroprotection via activation of adenosine triphosphate-regulated potassium channels after focal cerebral ischemia in rats. Anesth Analg. 2003;96:233–7.
27. Matsumoto S, Matsumoto M, Yamashita A, Ohtake K, Ishida K, Morimoto Y, et al. The temporal profile of the reaction of microglia, astrocytes, and macrophages in the delayed onset paraplegia after transient spinal cord ischemia in rabbits. Anesth Analg. 2003;96:1777–84.
28. Halsey JH Jr, Conger KA, Garcia JH, Sarvary E. The contribution of reoxygenation to ischemic brain damage. J Cereb Blood Flow Metab. 1991;11:994–1000.
29. Petito CK, Morgello S, Felix JC, Lesser ML. The two patterns of reactive astrocytosis in postischemic rat brain. J Cereb Blood Flow Metab. 1990;10:850–9.
30. Li Y, Chopp M, Zhang ZG, Zhang RL. Expression of glial fibrillary acidic protein in areas of focal cerebral ischemia accompanies neuronal expression of 72-kDa heat shock protein. J Neurol Sci. 1995;128:134–42.
31. Yamashita K, Vogel P, Fritze K, Back T, Hossmann KA, Wiessner C. Monitoring the temporal and spatial activation pattern of astrocytes in focal cerebral ischemia using in situ hybridization to GFAP mRNA: comparison with sgp-2 and hsp70 mRNA and the effect of glutamate receptor antagonists. Brain Res. 1996;735:285–97.
32. Schwartz JP, Nishiyama N. Neurotrophic factor gene expression in astrocytes during development and following injury. Brain Res Bull. 1994;35:403–7.
33. Kakinuma Y, Hama H, Sugiyama F, Yagami K, Goto K, Murakami K, et al. Impaired blood–brain barrier function in angiotensinogen-deficient mice. Nat Med. 1998;4:1078–80.
34. Nawashiro H, Brenner M, Fukui S, Shima K, Hallenbeck JM. High susceptibility to cerebral ischemia in GFAP-null mice. J Cereb Blood Flow Metab. 2000;20:1040–4.
35. Saadoun S, Papadopoulos MC, Watanabe H, Yan D, Manley GT, Verkman AS. Involvement of aquaporin-4 in astroglial cell migration and glial scar formation. J Cell Sci. 2005;118:5691–8.
36. Matsui T, Mori T, Tateishi N, Kagamiishi Y, Satoh S, Katsube N, et al. Astrocytic activation and delayed infarct expansion after permanent focal ischemia in rats. Part I: enhanced astrocytic synthesis of s-100β in the periinfarct area precedes delayed infarct expansion. J Cereb Blood Flow Metab. 2002;22:711–22.
37. Tateishi N, Mori T, Kagamiishi Y, Satoh S, Katsube N, Morikawa E, et al. Astrocytic activation and delayed infarct expansion after permanent focal ischemia in rats. Part II: suppression of astrocytic activation by a novel agent (*R*)-(–)-2-propyloctanoic acid (ONO-2506) leads to mitigation of delayed infarct expansion and early improvement of neurologic deficits. J Cereb Blood Flow Metab. 2002;22:723–34.
38. Ribeiro Mde C, Hirt L, Bogousslavsky J, Regli L, Badaut J. Time course of aquaporin expression after transient focal cerebral ischemia in mice. J Neurosci Res. 2006;83:1231–40.
39. Kaur C, Sivakumar V, Zhang Y, Ling EA. Hypoxia-induced astrocytic reaction and increased vascular permeability in the rat cerebellum. Glia. 2006;54:826–39.